Statistical analysis of the interaction between wind-waves and currents during early wave generation

Statistical analysis of the interaction between wind-waves and currents during early wave generation

L. Chiapponi[a], F. Addona[a], P.D. Carrasco[b], M.A. Losada[b], S. Longo[a]

[a]*Department of Engineering and Architecture, University of Parma, Parco Area delle Scienze, 181/A, 43124 Parma, Italy*
[b]*Instituto Interuniversitario de Investigación del Sistema Tierra, Universidad de Granada, Avda. del Mediterráneo s/n, 18006 Granada, Spain*

Abstract

We present the experimental analysis of the interaction between wind waves and currents, during the generation process, through laboratory experiments in a wind-waves-current tunnel. The objective is the quantification of the effects of a co-/counter-current on the main characteristics and statistical estimators of the wave field. Twenty-two experiments were performed with two different wind speed values and eleven different current speed values (including zero values, absence of current), with a ratio of current speed to group celerity $u_c/c_g \in [-0.47, +0.30]$, measuring the instantaneous water level in different sections with ultrasonic probes. The collected data allow the characterization of the free surface statistics, the calculation of the phase and group celerity of the waves, the analysis of the grouping. The aim is the description of the complex interaction between different forcing terms effective during wave generation. We found that (i) spectral shape and evolution is extremely sensitive to tiny counter-currents, with a fast grows of a second peak, (ii) grouping and the statistics of the free surface reflect the action of the current; (iii) energy transfer and breaking are significantly affected by the currents. The results are new and original and represent a set of data for understanding the generation of waves by the wind in all conditions in which the currents are not negligible, for example in the surf zone, lagoons, estuaries, swamps, shallow lakes and shallow reservoirs.

Keywords: wind-generated waves, currents, grouping, laboratory experiments

1. Introduction

The interaction between wind generated waves and currents is quite frequent in many natural and artificial environments, such as lakes, lagoons and reservoirs. In these areas there are often currents generated by tides, estuarine inlets, thermal and density effects, while sea and land breezes act cyclically generating waves. A frequent scenario is that of a wind that blows and generates free surface gravity waves (sea waves) in the absence of swelling and in the presence of current.

The applications of practical interest are the most varied. Sclavo *et al.* [1] explored the interaction of surface gravity waves and oceanic currents and how they influence bottom sediment dispersal and bathymetry evolution in the shallow northern Adriatic Sea (namely Gulf of Venice); Chiapponi *et al.* [2] analysed the wave-current interaction in the Porto di Lido entrance of the Venice Lagoon in order to evaluate the wave climate and the harbour tranquillity of a planned landing cruise. More recently, Melito *et al.* [3] studied the propagation of infragravity waves up the Misa river (Senigallia, Italy) during storm conditions.

The first aspect and starting point is wind wave generation. The process of energy transfer from the wind to the water waves has been widely discussed and debated by many researchers: Phillips [4] suggested that waves growth at the initial stage is generated by the resonance between atmospheric turbulent pressure fluctuations and perturbation of water surface; the Miles' theory [5] for wind wave growth, later on was extended by Miles [6], Phillips [7], Janssen [8] and Miles [9] to include viscous and turbulent effects. A validation of this theory is reported by Hristov *et al.* [10] in the field, and by Grare *et al.* [11] in the laboratory. Liberzon & Shemer [12] provided as comprehensive as possible set of experimental data that are valuable for comparison with theoretical models. Longo [13] measured in a systematic way wind and water waves in a wind tunnel with a water tank inside: he found that the phase celerity of the waves, affected by the current in the tank flowing in the opposite direction of wind action and of waves propagation, by wind drift and Stokes current, was larger than the theoretical celerity in the absence of the current. The group celerity was changed in a similar way, and a model was developed to account for the relative variation of phase celerity and group celerity, which includes a dependence of the drift velocity on the wave steepness. Further details on the turbulence structure for the

same experiments are given in Longo *et al.* [14, 15].

A second relevant aspect is the interaction of mechanically generated waves and currents. Van Hoften & Karaki [16] measured the wave amplitude attenuation along a laboratory wave channel to compare wave dissipation with and without flow. They found that energy is extracted from the waves, diffused downward and ultimately dissipated with an increment of bottom shear stress. Grant & Madsen [17] developed an analytical theory to describe the combined motion of waves and currents and the associated boundary shear stress in the vicinity of a rough bottom. Kempt & Simons [18, 19] presented the first extensive experimental program to investigate the interaction between gravity waves and a turbulent current. Changes induced in the mean-velocity profiles, turbulent fluctuations, bed shear stresses and wave attenuation rates were considered for a range of wave heights, keeping the wave period constant. Groeneweg & Klopman [20] presented a generalized Lagrangian mean formulation (GLM) to describe changes of the mean-velocity profiles in the combined wave-current motion. Many other researches focussed on the structure of the flow due to the interaction between waves and currents (Sleath [21], Klopman [22, 23], Umeyama [24], Smith [25], Roy *et al.* [26]).

A third aspect is energy dissipation due to breaking in the presence of currents, and frequency downshift due to nonlinear interaction. The energy dissipation due to current-limited wave breaking in monochromatic and random waves was studied experimentally by Chawla & Kirby [27, 28]. They observed that opposing current slows down the waves, leading to an increase in the wave steepness which sometimes leads to wave breaking. The waves get blocked when the current is strong enough to prevent the wave energy from travelling upstream, i.e. when the group celerity c_g goes to zero. For the largest wave amplitudes the wave energy shifts to a lower frequency due to side band instabilities, and the waves do not get blocked. Suastika *et al.* [29] performed laboratory experiments of wave blocking with periodic and random waves, with partial and complete wave blocking. They successfully identified the incident and reflected components of the wave thanks to an analysis in the frequency-wave number space. Ma *et al.* [30] experimentally studied in a wave-current flume the nonlinear evolution of regular waves in the presence of opposing current, observing downshift even with very small initial steepness. The downshift was generally gradual and occasionally

abrupt. Long & Huang [31] used a laser probe in order to measure the slopes of wind waves generated on both co- and counter-currents. The data were processed to yield an average wave-slope spectrum and it was found that the peak frequency and the intensity of the spectra were strongly influenced by the current. Zou & Chen [32] studied the wind and current effects on extreme waves formation and breaking. They combined a Navier−Stokes solver with the Smagorinsky subgrid-scale stress model and volume of fluid (VOF) air–water interface capturing scheme, comparing the model predictions to some laboratory experiments: the wave breaking location and intensity are modified by the following and opposing wind in a different fashion.

An entire body of literature has been devoted to the effects of currents on the statistics of waves, focussed on the appearance of rogue waves triggered when waves enter a field of opposing current (Onorato *et al.* [33]). Experiments in a wave tank showed that in the tertiary wave interaction the growth of the infinitesimal wave is reduced by a background current field (opposing and coflowing current conditions), more as an effect of the variability rather than for the presence of a mean current [34]. An adverse current gradient triggers modulational instability and, unless breaking induced by three-dimensional effects stops the process, the waves develop the maximum amplification. A strongly non-Gaussian statistics of the free surface elevation is favoured, with enhanced probability of extreme waves: the effect is stronger for unidirectional waves, but is evident also in the presence of directionality of the sea states [35, 36, 37, 38]. In passing, experiments on wave propagation in counter-current have been used as analog model of Hawking effect [39].

With the exception of some field observations (Lambrakos [40], Wolf & Prandle [41], van der Westhuysen [42] and Viitak *et al.* [43]), there is a scarcity of studies of the coupling between growing wind waves and currents. The interaction depends on the regime: at low wind speed, capillary waves are generated by the fluctuations in air pressure due to the corresponding fluctuations in the wind stream; then for increasing speed the wind boundary layer becomes turbulent and rhombic cells are formed and, for larger wind speed, wave breaking occurs and gravity replaces the surface tension as a key parameter for the wind-wave interaction. This interaction is affected by the presence of currents: currents change the effective wind because of the different relative velocity between the air and water with respect to the case of water at rest. Once formed and freely propagating like swell, the waves are refracted by currents (as well as by bathymetry changes). Near the coasts,

where current gradients often increase, refraction may be stronger and the angle wave-current is spatially non-homogeneous. When current and waves are in the same direction, the result is the lengthening of waves and the reduction of wave heights. On the other hand, the waves are shortened and steepened by an opposing current, often to the extent of inducing breaking.

The previous arguments and most of the above-mentioned studies, are for long-crested waves. Short-crested waves interacting with rip currents were recently studied by Wei *et al.* [44]. They found that (i) the non-linear interaction between intersecting waves, and (ii) the interaction between rip current and short-crested wave crest, generate isolated waves propagating shoreward with an increased wave celerity. Hedges *et al.* [45] developed a theoretical model to describe the interaction of short-crested random waves with large-scale currents, with the prediction of the transformed spectral densities using the principle of wave action conservation.

As a matter of evidence the topic is variegate and with several possible combinations of wind, current, swell, bathymetry changes, breaking. The review by Cavaleri *et al.* [46] depicts the numerous aspects already interpreted and the still open questions. In order to clarify some aspects of these phenomena, a series of tests were carried out in a wind wave current tank. In these tests, gravity waves are generated in a laboratory only by the wind, with currents flowing in the same or opposite direction of the waves (co-current and counter-current, respectively). The main aim is the analysis of the evolution of the waves in terms of statistical indicators in time and frequency domains.

This manuscript is organized as follows. In §2 the experimental apparatus and the measurements procedures and protocols are described. In section §3 the experimental results on water waves are presented and discussed, with a focus on the phase and group celerities. Wave grouping is analysed in §4. The conclusions are presented in §5. In Appendix A the relevant dimensionless groups are described and the scaling rules are discussed.

2. Experimental set-up

The experiments were conducted in the Atmosphere-Ocean Interaction Flume (CIAO) at IISTA (Instituto Interuniversitario de Investigación del Sistema Tierra en Andalucia), shown in Figure 1. The CIAO is a wave fume 1.0 m wide and 16.0 m long, designed for a water depth of 70 cm. The flume has a paddle at each of its ends, which allow the generation of regular up to

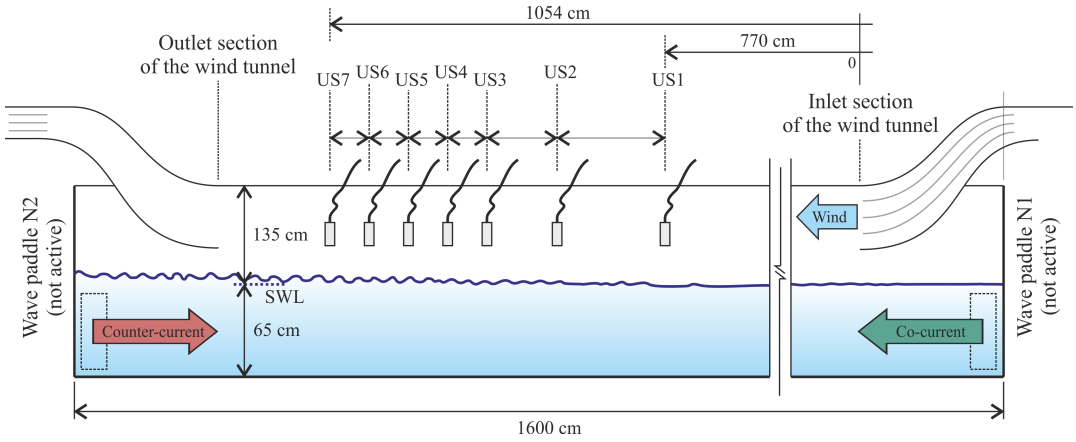

Figure 1: The experimental flume adopted for the tests, with the representation of the Ultrasonic probes (US1-7) located in the measurement sections, $x_{\text{US1-7}} = 770, 920, 993, 1008, 1024, 1042, 1054$ cm.

second order and irregular waves with period from 1 to 5 s and height up to 25 cm. A closed-circuit wind-generation system (wind tunnel) with wind speed up to 12 $\mathrm{m\,s^{-1}}$ directly generates waves with an effective fetch length approximately equal to 10 m. A current generation system allows currents up to 0.75 $\mathrm{m\,s^{-1}}$. For the present activity, waves were generated by wind with a free stream velocity, $U_{w\infty}$, equal to $7.4 - 10.8$ $\mathrm{m\,s^{-1}}$ (low wind speed, LWS, and high wind speed, HWS, respectively). In both conditions the generation of waves was initially observed without current and then with co- or counter-current. Seven UltraLab ULS 80D acoustics wave gauges were employed for water level measurements along the flume, with a maximum repetition rate equal to 75 Hz, a vertical resolution of ≈ 0.5 mm and a reproducibility of $\pm 0.15\%$. The level signals were acquired for at least 600 s with a data rate of 100 Hz. Measurements of the wind speed were performed with a Pitot tube in the section 9.95 m away from the wave paddle N1 (both paddles are not used for the present tests). The velocity profile in the water side was measured in the absence of current with a two-component Laser Doppler Velocimeter by TSI. Figure 2 shows the flume during one of the tests. The mean velocity of the currents (measured without wind and waves) was estimated with a micro-propeller meter for a given rotation rate of the pump, see the velocity profile shown in Figure 3*a*. Considering that the installation allows to precisely control the pump rotation rate, and that during the experiments there were no significant variations of the hydraulic resistances of the circuit, a high

reproducibility of the flow discharge is guaranteed by fixing the rotation rate of the pump. For this reason, the velocity measurements were not repeated during the tests to prevent local disturbances in the fluid domain. The main parameters of the experiments are listed in Table 1.

Exp.	$U_{w\infty}$ ($\mathrm{m\,s^{-1}}$)	u_c ($\mathrm{cm\,s^{-1}}$)	N_{waves} #	T_{rms} (s)	H_{rms} (mm)	$a_{c\,rms}$ (mm)	$a_{t\,rms}$ (mm)	$H_{1/3}$ (mm)	u_c/c_g	H_{rms}/L	Re_w
21	7.4	0	1770	0.34	17.0	8.6	8.6	22.7	0.00	0.062	1300
1	7.4	-4	1292	0.46	21.2	11.2	10.7	29.3	-0.06	0.056	1700
2	7.4	-9	1209	0.50	21.2	11.1	10.5	29.5	-0.10	0.054	1500
3	7.4	-13	1082	0.55	25.9	13.7	12.6	36.2	-0.13	0.045	2100
4	7.4	-17	952	0.63	28.4	15.0	13.9	39.7	-0.11	0.032	2200
5	7.4	-21	791	0.76	39.3	20.8	19.0	54.0	-0.24	0.084	3500
16	7.4	4	2109	0.28	14.4	7.4	7.3	19.7	0.05	0.086	1200
17	7.4	9	2179	0.27	14.5	7.4	7.4	19.9	0.10	0.061	1200
18	7.4	13	2342	0.26	13.0	6.6	6.7	17.9	0.14	0.067	1000
19	7.4	17	2401	0.25	11.7	6.0	6.0	16.2	0.12	0.054	900
20	7.4	21	2505	0.24	10.0	5.2	5.2	13.8	0.22	0.080	700
22	10.8	0	1339	0.45	32.6	17.6	15.4	43.8	0.00	0.076	4300
6	10.8	-4	1085	0.55	40.1	22.1	18.9	55.1	-0.04	0.072	5500
7	10.8	-9	888	0.67	40.7	22.3	19.8	56.1	-0.08	0.071	4600
8	10.8	-13	863	0.69	41.5	22.9	19.9	56.7	-0.11	0.064	4700
9	10.8	-17	890	0.67	43.0	23.5	20.2	59.2	-0.21	0.062	5100
10	10.8	-21	801	0.75	54.2	29.0	25.8	75.0	-0.26	0.064	7000
11	10.8	4	1573	0.38	29.9	16.1	14.2	40.1	0.05	0.060	4200
12	10.8	9	1629	0.37	28.6	15.3	13.7	38.4	0.10	0.053	3900
13	10.8	13	1713	0.35	27.2	14.5	13.1	37.0	0.15	0.045	3700
14	10.8	17	1736	0.35	27.2	14.4	13.1	36.8	0.25	0.073	3700
15	10.8	21	1785	0.34	25.8	13.8	12.5	35.4	0.24	0.081	3500

Table 1: Parameters of the tests. $U_{w\infty}$ is the wind asymptotic velocity, u_c is the depth-averaged current velocity, positive if coflowing and negative if counter-flowing condition, N_{waves} is the number of waves detected in the record with a zero-crossing analysis, T_{rms} is the root mean square wave period, H_{rms}, $a_{c\,rms}$, and $a_{t\,rms}$ are the root mean square values of the wave height, of the crest and of the troughs, $H_{1/3}$ is the one-third wave height, c_g is the group celerity, Re_w is the Reynolds number for the water side near the free surface. Data refer to section US3.

In order to check if the waves are in intermediate or deep water, Figure 3*b* shows the relative depth h/L for all the experiments. Since $h/L > 0.5$ for all tests, the waves propagate in deep water.

Figure 2: A picture of the flume during tests.

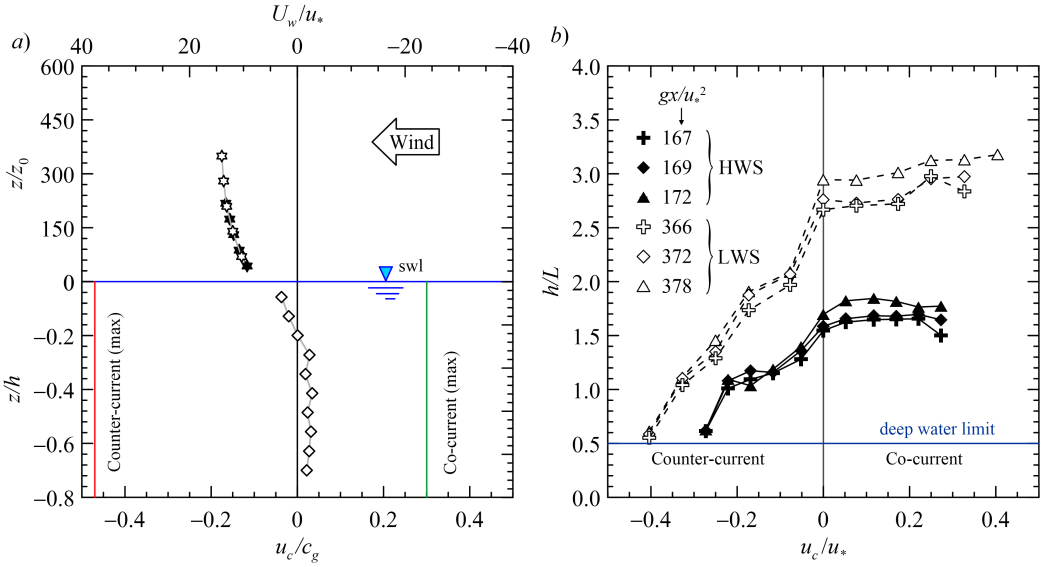

Figure 3: *a*) Velocity profiles, air side (✡) and water side (◇), measured in the absence of imposed currents. The green/red lines refer to the minimum and maximum depth-averaged velocity of the co-/counter-currents during the experiments. U_w is the wind velocity, u_c is the current velocity, u_* is the friction velocity of the wind, c_g is the group celerity of the waves, h is the mean water depth, z_0 is the roughness length. *b*) Relative depth h/L for tests at different current speed.

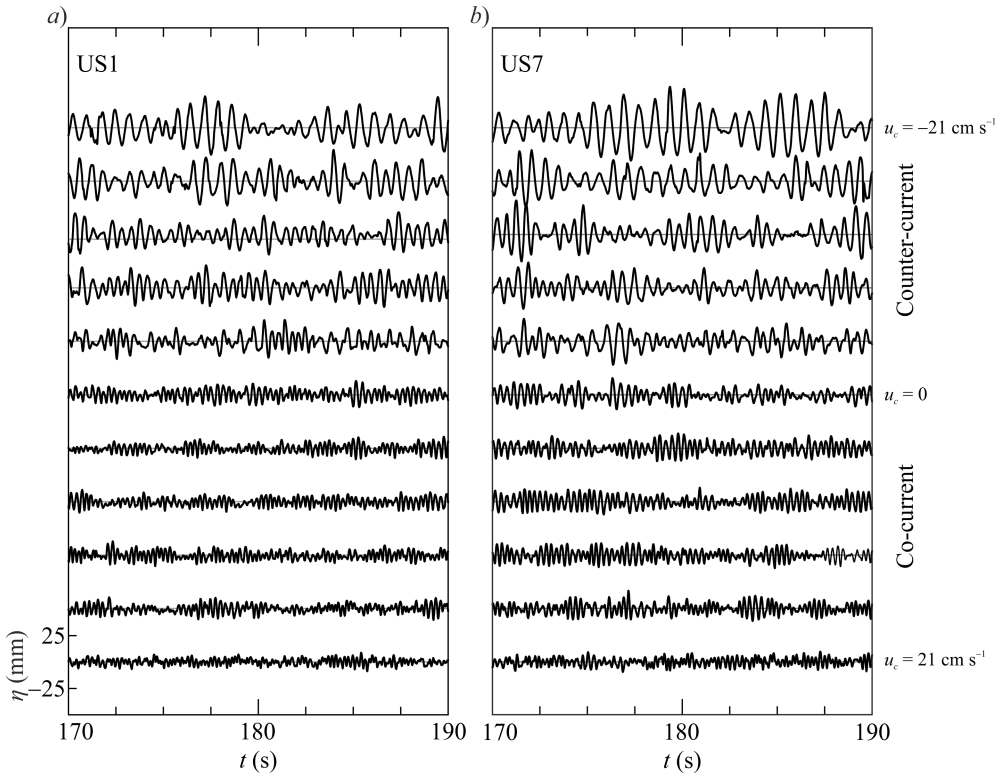

Figure 4: Time series of the free surface elevation for LWS tests. *a*) Data at section US1 (minimum fetch), *b*) data at section US7 (maximum fetch).

3. Experimental results

3.1. Wave statistics in the time domain

Figures 4–5 show the water surface time series at section US1 and US7 for LWS and HWS tests, respectively, with evident differences between tests with different current velocity. The abrupt modifications due to a small counter-current are evident, with a progressive increment of the wave period for increasing speed of the counter-current.

The instantaneous water surface elevation data were elaborated by applying a phase-average operator, defined as

$$\widetilde{\eta}(t) = \frac{\sum_{i=1}^{N_p} \eta(t + iT_p)}{N_p}, \tag{1}$$

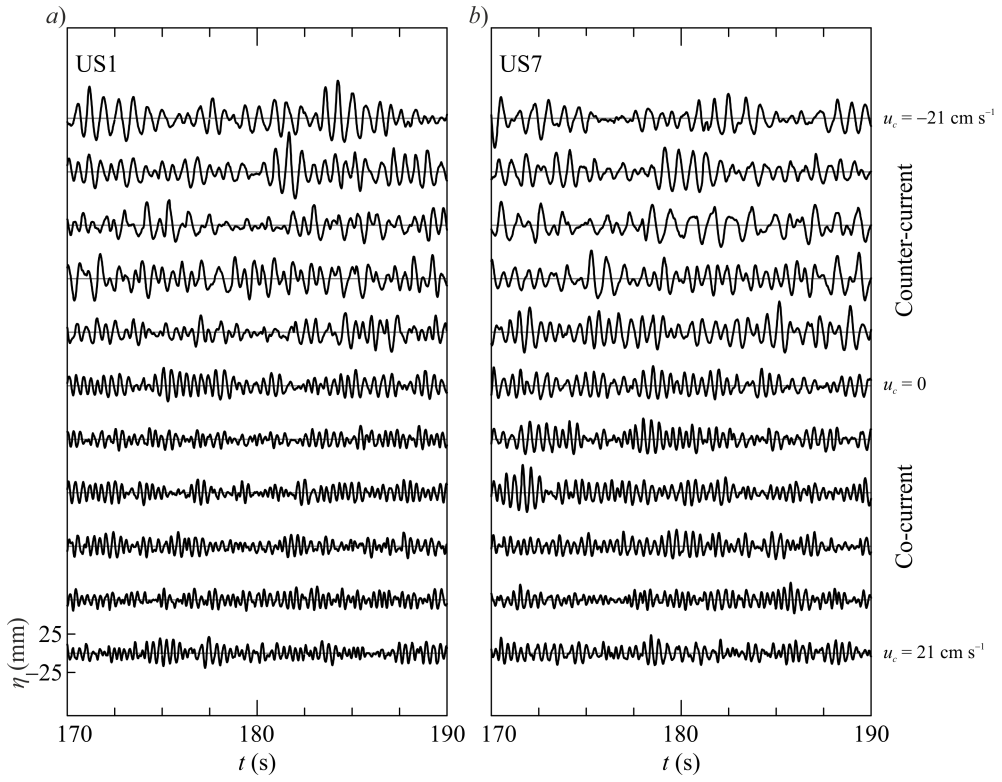

Figure 5: Time series of the free surface elevation for HWS tests. *a*) Data at section US1 (minimum fetch), *b*) data at section US7 (maximum fetch).

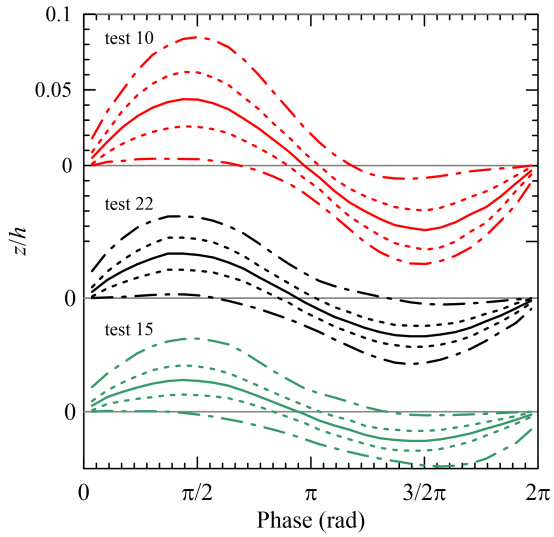

Figure 6: Phase-averaged surface elevation at section US3 for test 10 ($u_c = -21$ cm s^{-1}), test 22 ($u_c = 0$) and test 15 ($u_c = 21$ cm s^{-1}), all in HWS conditions. The dashed lines indicate ± 1 standard deviation, the dash-dotted lines indicate the maximum and minimum level recorded during the experiment.

where $T_p \equiv 1/f_p$ is the peak period of the spectrum and N_p (see §3.2 for details on spectral analysis) is the number of waves characterized by a period in the interval $T_p(1 \pm 5\%)$. Figure 6 shows the results for three experiment in HWS conditions: a co-current results in a smoothing of the wave, with respect to the absence of current, while a counter-current induces a growth in wave height and a higher value of the standard deviation, which indicates a greater variability of the observed profiles. In counter-current also the maximum/minimum levels of the waves are larger than in co-current, coherently with a wave statistic highly affected by the opposing flow [30].

The data were analysed with a mean level up-crossing technique, obtaining the wave height H, the wave crest a_c and trough a_t amplitudes listed in Table 1 and depicted in Figure 7 for the tests without currents. The results indicate a monotonic increase in the wave height with fetch, and a fairly good symmetry of the waves in LWS and for large fetch, but with crests being higher than troughs for HWS tests. The HWS tests reach very fast the asymptotic trend with $H \propto x^{0.6}$ and the LWS tests show an initial faster growth followed by a region with constant growth rate with $H \propto x^{0.4}$. Hasselmann *et al.* [47] proposed $H \propto x^{0.5}$ for short fetches.

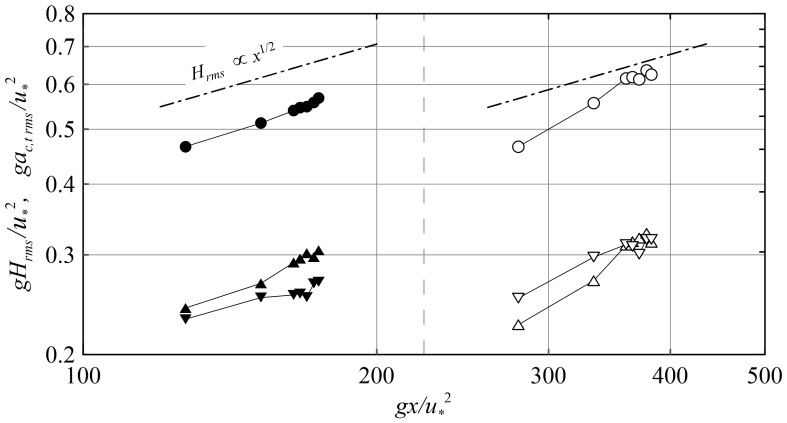

Figure 7: Wave evolution with non-dimensional fetch in the absence of currents: test 22 (HWS condition, $U_{w\infty} = 10.8$ m s^{-1}, solid symbols) and test 21 (LWS condition, $U_{w\infty} = 7.4$ m s^{-1}, empty symbols). Root mean square values of the wave height (●, ○), wave crest a_c (▲, △) and wave trough a_t (▼, ▽).

Figure 8*a* shows the wave evolution in the presence of co- and counter-current, and Figure 8*b* shows the same data in terms of variation of the wave height with respect to the wave height measured in section US1, the smallest fetch. In co-current conditions the evolution of the waves with fetch length is regular, with wave height generally decreasing for increasing speed of the current. For increasing co-current the growth rate exponent in HWS decreases from 0.6 to a minimum of 0.2. In LWS the growth rate for varying current speed is less regular, and reaches a minimum value 0.38.

In counter-current conditions the evolution of the waves is highly irregular, with decay beyond a given fetch length and with a dispersion of the data. In LWS, the growth rate is definitely negative beyond a given fetch, reaching the value of -2.6 for the strongest counter-current speed. This phenomenon is mainly attributed to the wave breaking which dissipates energy in excess with respect to the energy transferred to the waves by the wind. Recent experiments by Toffoli *et al.* [38] have demonstrated the destabilising effect of the counter-current on mechanically generated waves, with deviations of the statistical properties favouring rogue waves and breaking: above the limiting condition $k_p h \to 1.36$, where k_p is the wave number corresponding to spectral peak, a direct cascade due to wave breaking occurs. In the present experiments $k_p h > \approx 5$, hence the mechanism of direct cascade of energy is always effective.

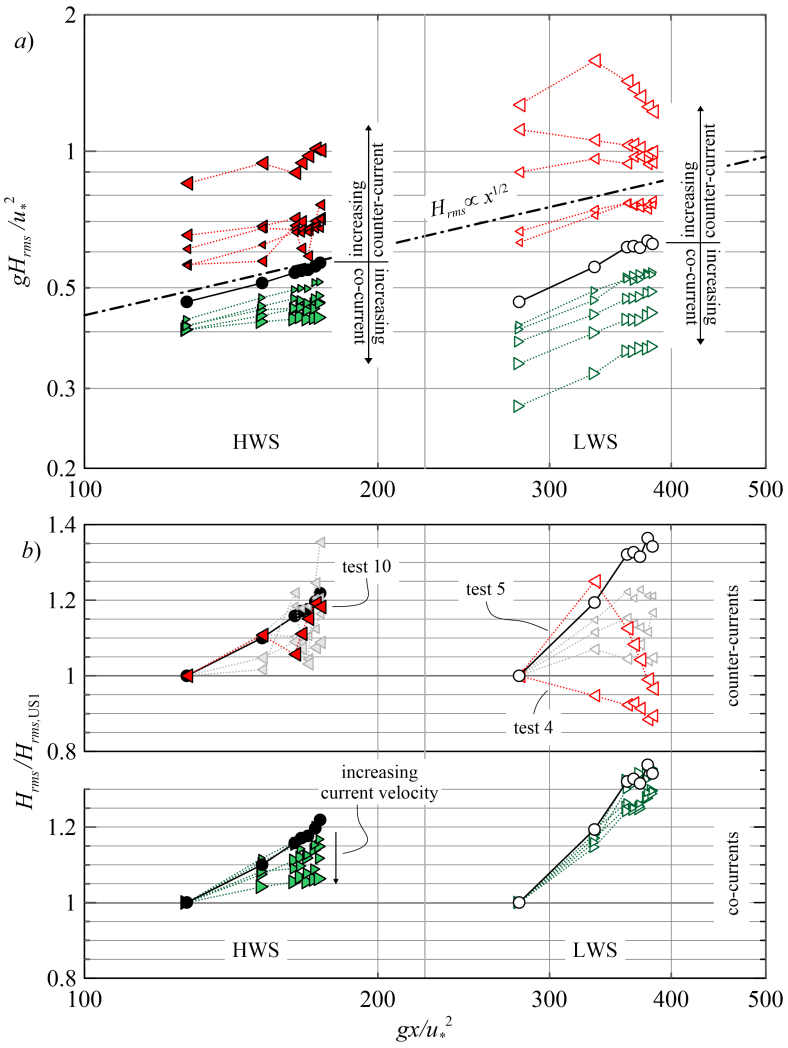

Figure 8: Wave evolution with fetch length. *a*) Dimensionless wave height H_{rms}; *b*) H_{rms} normalized with respect to its value measured in section US1. Filled symbols refer to high wind speed condition, $U_{w\infty} = 10.8\ \mathrm{m\,s^{-1}}$, empty symbols refer to low wind speed condition, $U_{w\infty} = 7.4\ \mathrm{m\,s^{-1}}$. ●, ○ no current; ▶, ▷ co-current; ◀, ◁ counter-current. The size of the symbols is proportional to the speed of the current.

Figure 9a shows the effect of the current on H_{rsm}. The wave height increases for decreasing average velocity of the current, with a minimum value for the maximum co-current speed, and maximum value for the maximum counter-current speed, according to the prediction by Longuet-Higgins & Stewart [48]. The scaling with u_c/c_g indicates non monotonic trends for the counter-current case, mainly for the LWS case. We remind that breaking, a candidate to explain this odd behaviour, is favoured for milder counter-current by the non-uniformity in the current flows [38]. The effects of the currents on the period gT_{rms}/u_*, are shown in Figure 9b. The wave period increases for decreasing current velocity, weakly for co-currents and strongly for counter-currents. The increasing of the wave period is the classical frequency downshift.

Figure 10a depicts the steepness H_{rms}/L for varying current speed and Figure 10b shows the kurtosis of the instantaneous free surface level, a classical indicator of the gaussianity of the field, assuming a value of 3 for a perfect Gaussian pdf. The wave steepness has a maximum for weak counter-currents and then decreases with the speed of the current for both co- and counter-current conditions. This behaviour is expected for co-current conditions, with increased wave length, but looks odd for a counter-current (except locally when breaking occurs): the wave height increases but the wave length increases even faster. The phenomenon is addressed to non-linear wave-wave interactions, responsible for the energy transfer towards lower frequency wave components [49]. The maximum steepness occurs at large fetch for mild counter-current, $u_c/c_g \approx -0.10, -0.15$, where the kurtosis shown in Figure 10b has a maximum. Steepness reduction in counter-currents is accompanied by a decreasing kurtosis (with a significant deviation from Gaussian statistics), whereas is accompanied by an increasing kurtosis in the presence of co-currents, although always less than 3.

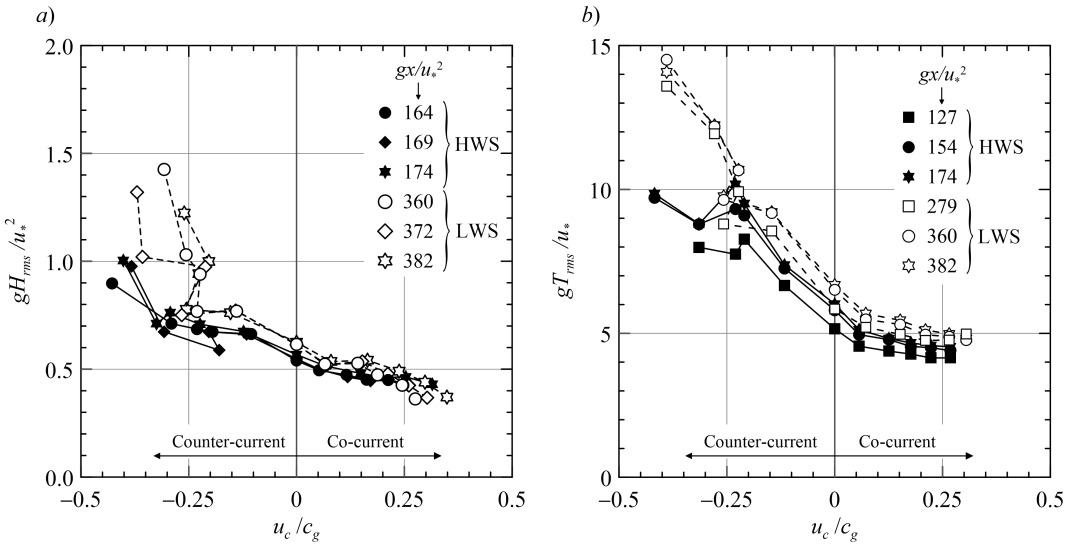

Figure 9: Wave properties at different fetches as a function of u_c/c_g. *a*) Wave height, and *b*) wave period. Empty and filled symbols refer to LWS and HWS tests, respectively.

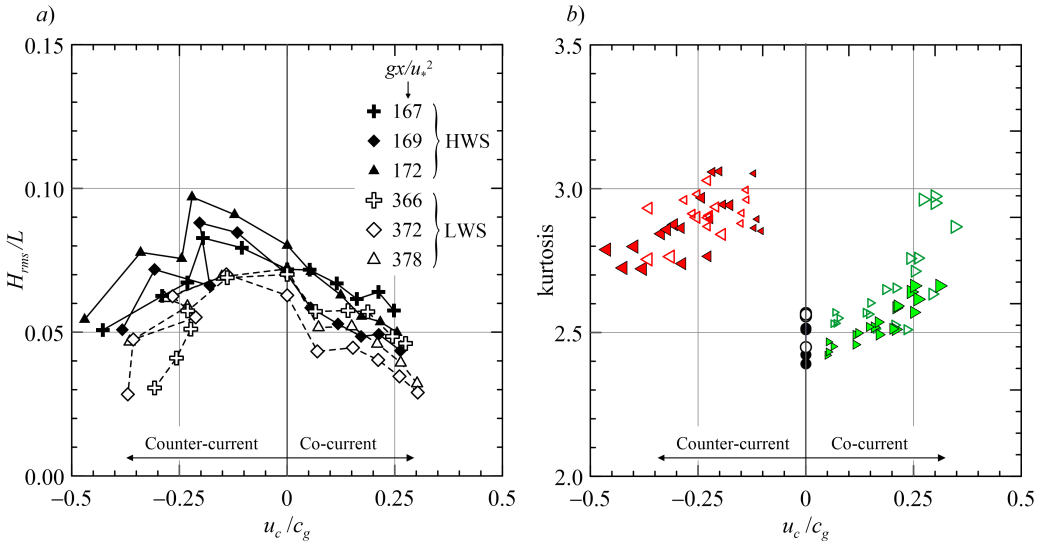

Figure 10: *a*) Wave steepness H_{rms}/L at different fetches as a function of u_c/c_g. Empty symbols and filled symbols refer to LWS and HWS tests, respectively. The curves connect the data for the same fetch. *b*) Kurtosis of the free surface elevation.

3.2. Wave statistics in the frequency domain

The power spectra of the free surface elevation are computed by means of a Welch's averaged, modified periodogram method, with a spectral resolution of 0.05 Hz and windows of 30 s with overlap of 50%, resulting in a bandwidth of 0.033 Hz and 78 degree of freedom for each spectral estimate.

Figure 11 shows the power spectra for the HWS condition at section US3, with a shape strongly affected by the current and with a peak shifted toward higher/lower frequencies for increasing speed of the co/counter-current, eventually with a secondary peak for counter-currents. In general the non linear transfer induces a downshift of the peak frequency even without counter-current, but the the presence of a counter-current induces a substantial and quick downshift of the peak, as already detected in the evolution of random mechanically generated wave fields [38].

Figure 12 shows the spectra for increasing fetch for three counter-current tests with HWS, starting from $u_c/c_g = 0$. A straight line refers to PSD $\propto f^{-4}$ and corresponds to the prediction of the weak wave turbulence theory [50]. The present experiments show steeper spectra $\propto f^{-6}$, as observed in other laboratory experiments [see 51, 52, 53]. We observe that in all tests there is a peak above $\approx$ 1 Hz, which become only one for the two conditions without current and with the maximum counter-current speed. For tests with moderate and progressively stronger counter-current, a second low-frequency peak appears at frequency slightly less than 1 Hz, which becomes dominant for tests with $u_c/c_g = -0.08; -0.11$. The variation of the spectrum shape with the fetch is quite evident for test in panel *d*): the low frequency peak at $\approx$ 0.9 Hz is stable in frequency and increases fourfold its value; the high-frequency peak slowly shifts to a lower frequency, slightly increases the width but without significant reduction. As a result, at short fetch the high frequency peak dominates, at long fetch it is the opposite.

It has been recently demonstrated that the growth of wind-waves in the generation phase is a strongly non-linear phenomenon [38], with a statistics prone to the generation of rogue waves. The presence of counter-current triggers modulational instabilities [33], in particular in the presence of a non-homogeneous counter-current field [37]. We expect that the presence of both forcing terms, i.e. a wind-wave generation field and a counter-current, enhances the instabilities and the non-linearity [38], and accelerates nonlinear energy transfer. The effects are more prominent for increasing values of u_c/c_g and, for mechanically generated waves, the maximum value of the kurtosis of the wave statistics in [38] was reached for $u_c/c_g = -0.25$. In the present

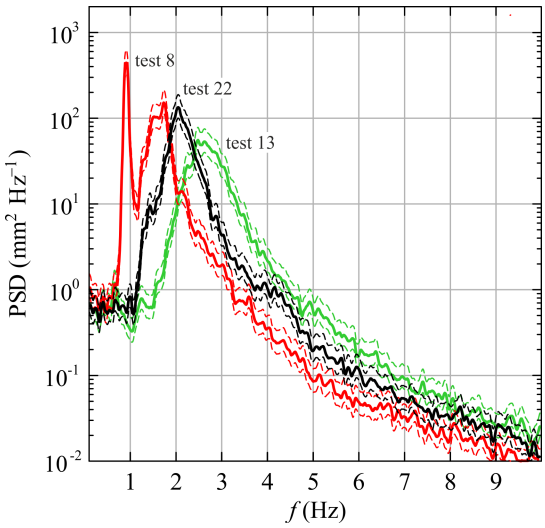

Figure 11: Power spectra of the free surface elevation at section US3. Test with co-current (test 13), without current (test 22), and with counter-current (test 8). Dashed curves are the 95% confidence limits.

tests we observe that the strongest variability is at $u_c/c_g \approx -0.11$, when the maximum spatial evolution of the power spectrum is observed, with an evident growth of the low-frequency peak which finally is more energetic than the high frequency one. The high frequency component does not vanish and remains almost constant. In comparing these spectral evolution we bear mind that a continuous influx of energy is due to the blowing wind, which partially hides the expected spectral evolution with a progressive growth of the low frequency component and a vanishing high frequency peak. We also notice that the relatively short fetch limits the observation of further evolution of the phenomena.

Figure 13 shows the spatial evolution of the spectra analysed in Figure 12. A tiny counterflow with $u_c/c_g = -0.04$ in panel b) is sufficient to favour the growth of a low frequency component. For stronger counter-current, the evolution is variegate, with a concentration of energy at $\approx$ 1 Hz for $u_c/c_g = -0.08$, followed by a reappearance of the peak at $\approx$ 1.5 Hz for $u_c/c_g = -0.11$ which becomes the most energetic peak for $u_c/c_g = -0.21$. In the strongest counter-current test, with $u_c/c_g = -0.26$, the low frequency peak disappears and the spectrum is again a single-peak spectrum with most of the energy at $\approx$ 1.25 Hz. In summary, the counter-current facilitates the growth of a low frequency contribution which shares the energy with the

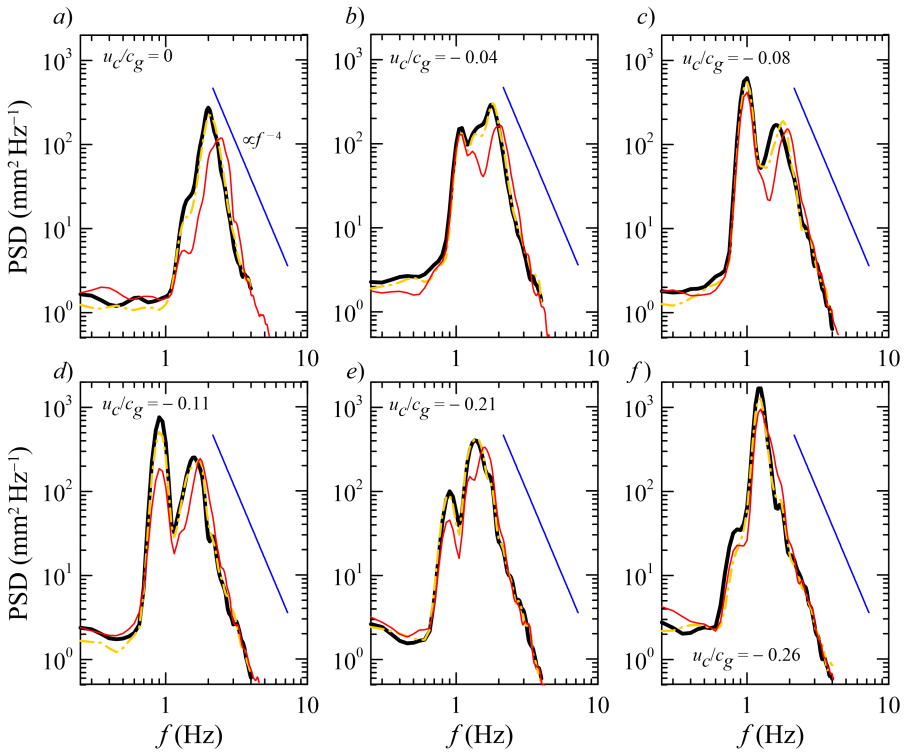

Figure 12: Power spectra of the free surface elevation for counter-current tests with HWS, $u_c/c_g = 0, -0.04, -0.08, -0.11, -0.21, -0.26$. Thin red curves refer to section US1, dash-dotted orange curves refer to section US3, and thick black curves refer to section US7, with fetch increasing from US1 to US7. See Figure 13 for the spatial evolution of the spectra.

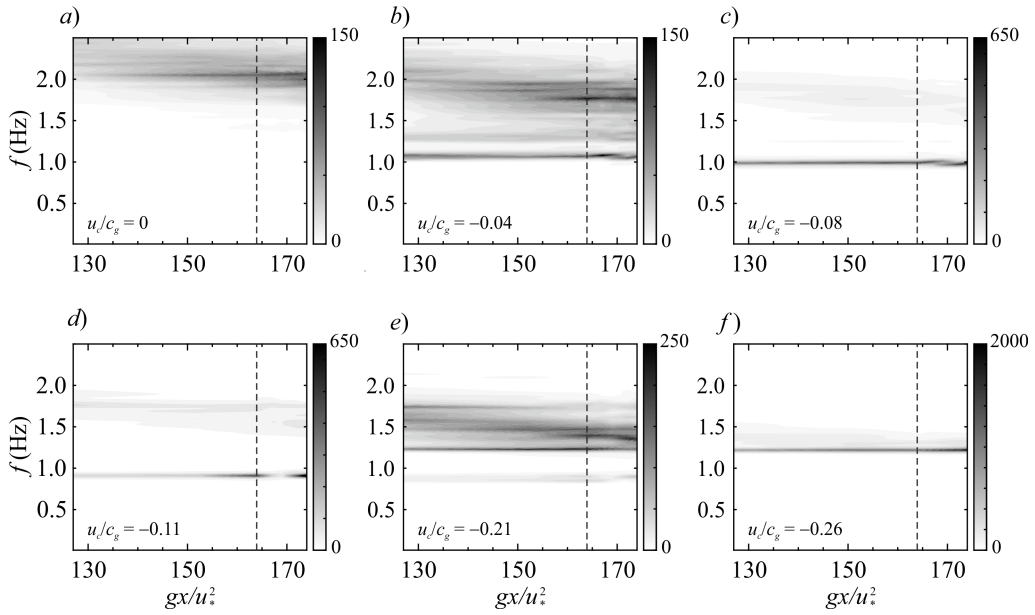

Figure 13: Fetch evolution of the power spectra of the free surface elevation for counter-current tests with HWS, $u_c/c_g = 0, -0.04, -0.08, -0.11, -0.21, -0.26$. Note that the scales of the colorbar are different for each test and have units $\mathrm{mm}^2\,\mathrm{Hz}^{-1}$. The dashed line represents section US3, see Figure 12.

original high frequency term, visible in the experiment without counter-flow. The transfer seems extremely sensitive to the speed of the counter-current.

The presence of a current highly affect the statistics of the wind generated waves, with changes in the statistical estimators and in the spectrum. The effects are significant if the ratio between the scales of the waves and of the current, e.g., the velocity and the group celerity, is of $O(10^{-1})$, see the analysis of celerity in §3.3.

3.3. Phase and group celerities of the waves

In the presence of uniform currents the following classical dispersion equation for gravity waves holds:

$$\omega - kU = \pm \left[\left(gk + \frac{\sigma}{\rho} k^3 \right) \tanh kh \right]^{1/2}, \qquad (2)$$

where $\omega = 2\pi/T$ is the angular frequency, T is the wave period, $k = 2\pi/L$ is the wave number, L is the wave length, ρ the water mass density, σ is

the surface tension. In the presence of wind drift Liberzon & Shemer [12] proposed an empirical dispersion relation,

$$c = c_0 \left(1 + ak + bk^2\right), \tag{3}$$

with $c_0 = \omega/k$ computed using the gravity capillary wave dispersion, a and b are fitting coefficients.

In the present experiments, even the longer waves propagate in deep water conditions, hence $\tan kh \approx 1$. Since the waves are not monochromatic, for computations we will refer to the dominant (most energetic) wave component.

The experimental phase celerity is estimated by the cross-correlation of the synoptic data recorded in two neighbour Ultrasound sensors. The average phase celerity between two sensors can be computed as

$$c_{ave} = \frac{\Delta x}{\tau}, \tag{4}$$

where Δx is the distance between two sensors and τ is the time delay of the highest peak of the cross-correlation function. The relative uncertainty in the estimate of the phase celerity is equal to

$$\frac{\mathrm{d}c_{ave}}{c_{ave}} = \frac{\mathrm{d}\Delta x}{\Delta x} + \frac{\mathrm{d}\tau}{\tau}. \tag{5}$$

The first contribution is due to the uncertainty in the probes positions and to the dispersion of the Ultrasound cone. By assuming $\mathrm{d}\Delta x = 4$ mm, it results $\mathrm{d}\Delta x/\Delta x \approx 3\%$. The second contribution is addressed to the uncertainty in locating the peak of the cross-correlation function, and can be computed according to Longo [13], giving a value of 1%. Therefore the overall uncertainty in phase celerity estimate is $\mathrm{d}c_{ave}/c_{ave} \approx 4\%$.

The results are shown in Figure 14 and are compared with eq.(2). An evident discrepancy is observed between experiments and theory, with minor differences when counter-current is present. On the opposite, in presence of a co-current the experimental phase celerity is in excess with respect to theory. This effect could be due to the drift currents induced by the wind and to the change in the velocity profiles caused by the wave motion [18, 19].

The theoretical group celerity is computed by differentiating the dispersion relation eq.(2):

$$c_g \equiv \frac{\partial \omega}{\partial k} = \frac{c}{2}\left(1 + \frac{2kh}{\sinh 2kh}\right) + U, \tag{6}$$

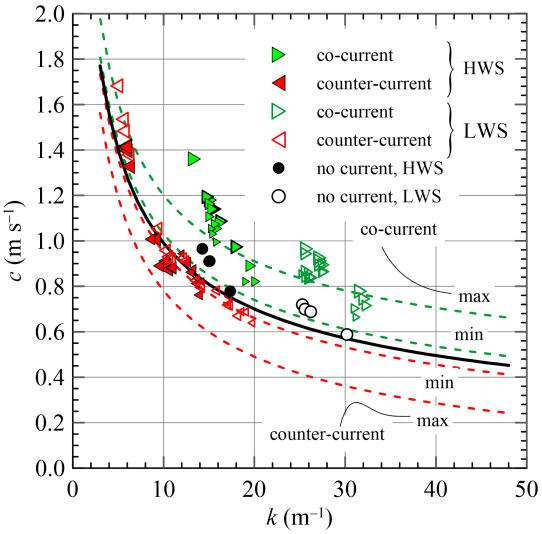

Figure 14: Phase celerity as a function of the wave number. The bold line is the dispersion relation without current, the dashed lines are the dispersion relation with current of different velocity, positive and negative. Empty and filled symbols refer to experiments in LWS and HWS conditions, respectively. The size of the symbols is proportional to the speed of the current.

and in deep water becomes

$$c_g = \frac{c}{2} + U, \tag{7}$$

where we have neglected capillarity.

The experimental group celerity can be estimated by the cross-correlation of the envelopes of the water levels measured in two neighbour sections. Under the hypothesis of narrow bandwidth signals, the same results can be achieved computing first the cross-correlation of the water level signals and then the Hilbert transform of the cross-correlation. The delay of the peak of the envelope, τ_g, yields the computation of the group celerity $c_g = \Delta x/\tau_g$ (Bendat & Piersol [54], Longo [13]). A comparison of the results obtained by adopting both methods are shown in Figure 15*a*. The error bars were estimated using the Monte Carlo method: the errors affecting both water levels and probes positions are supposed to have a Gaussian distribution. For each test, 10 000 random realizations of these variables were generated and the group celerity was estimated, producing a new population which also have Gaussian distribution. The mean value of the distribution represents the estimated value of c_g, while the standard deviation of the population is

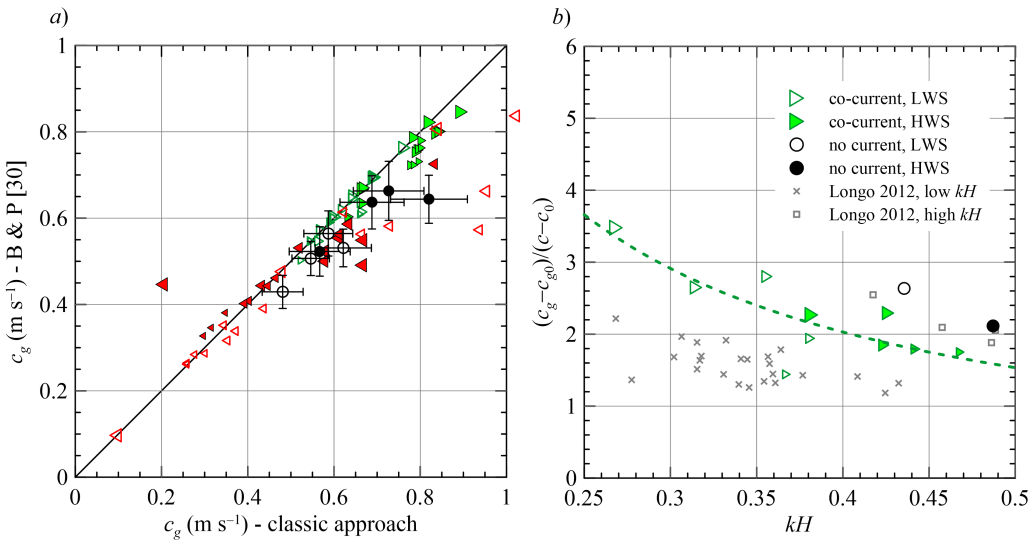

Figure 15: *a*) Group celerity, comparison between two different computational methods. Filled symbols refer to HWS and empty symbols refer to LWS condition, respectively. The size of the symbols is proportional to the speed of the co/counter-current, circles refer to the absence of current. The bold line is the perfect agreement. *b*) Ratio between group and phase celerity excesses. Filled symbols refer to HWS condition, empty symbols refer to LWS condition. The size of the symbols is proportional to the speed of the co- or counter-current. The dashed line is the theoretical model (Longo [13]) fitted for steep waves.

assumed to be the uncertainty of the estimate. The results from the two approaches are comparable for almost all tests, with differences appreciable and sometime relevant (up to 25%) in presence of a strong counter-current. This behaviour is due to the modification of the spectrum shape induced by counter-currents, which are responsible for a faster transition towards a double peak spectrum. The method from Bendat & Piersol reduces the uncertainty by approximately 15%, since the group celerity is obtained by applying only a cross-correlation and the envelope algorithms, instead of the classical method, by calculating two envelopes and one cross-correlation. Results are similar for probes that are faraway, like probes in sections US1 and US2.

Focusing on the energy propagation, it is known that the theoretical kinematic limit is reached if there is an adverse uniform current exceeding $1/4c_0$, where c_0 is the phase celerity without current. This limit is equivalent to $u_c/c = -1/2$, a convection velocity equal and opposite to the group celer-

ity in deep water, $u_c/c_g = -1$, hence energy cannot propagate (Phillips, [7], where it is also shown that wave breaking appears earlier than forecast by the kinematic limit). In the present study, when counter-currents are present, the experimental group celerity is generally lower than in the absence of currents; however a clear trend can not be detected, presumably as a consequence of breaking which dissipates energy along the channel in a way that can not be easily predicted.

The ratio between group and phase celerity excesses (both calculated with respect to the theoretical values in the presence of the current) is shown in Figure 15*b* as a function of the wave steepness. The wind drift and the Stokes current are both variable in space, but we observe that they affect the phase and the group celerities in a similar way when co-currents are present, with a ratio between the excesses equal to one. We remind that in the absence of currents the variation $(c_g - c_{g0})$ is greater than $(c - c_0)$. The experimental evidence is interpreted by the model proposed by Longo [13], based on the assumption that the group celerity excess differs from the phase celerity excess as a monomial function of the wave steepness:

$$\frac{c_g - c_{g0}}{c - c_0} \equiv \frac{\bar{u}_s + kH\left[\mathrm{d}\,\bar{u}_s/\mathrm{d}\,(kH)\right]}{\bar{u}_s} = f\,(kH)\,, \quad \text{with} \quad f(kH) = r \cdot (kH)^{\beta}\,, \tag{8}$$

where $\bar{u}_s$ represents the surface drift, r and β are an empirical coefficient and exponent, respectively. The integration of eq.(8) yields an exponential function

$$\frac{\bar{u}_s}{\bar{u}_{sr}} = \frac{k_r H_r}{kH} \exp\left[\frac{r}{\beta}\left(\frac{kH}{k_r H_r}\right)^{\beta} - 1\right], \tag{9}$$

where $\bar{u}_{sr}$ is the drift speed in the section where the steepness is $k_r H_r$. The parameters of the interpolation are $r = 0.64$ and $\beta = -1.25$, close to the values reported in Longo [13] for steep waves ($r = 0.62$ and $\beta = -1.60$). The data in the presence of counter-current (not shown) appear too disperse (also as a consequence of an almost null value of $(c - c_0)$), and no general conclusions can be drawn for this condition.

4. Wave grouping

Although sea waves may look random, the analysis of wave records reveals that high waves appear in group rather than individually. The grouping of high waves has practical implications of great interest since it can influence,

e.g. (i) the effective number of consecutive waves necessary to produce resonance in structures, (ii) the stability blocks of sloping breakwaters, and (iii) the efficiency of seawalls against the wave overtopping (see, e.g., Goda [55]). For small waves, grouping is relevant since long wave-groups can easily be reflected raising the level of vertical mixing. We expect that grouping is still present for wind waves and currents coexisting and interacting.

Low-grazing-angle radar imaging of wind waves have suggested grouping effects for a developing sea in deep water, with groups modulating the occurrence of wave breaking [56]. Experiments have also shown that wind-wave energy is strongly suppressed in presence of a modulated wave train [57]. Benjamin-Feir instabilities lead to groups, hence the analysis of the groups gives hints on the statistics of the free surface elevation, on breaking processes, on wind waves growth. The effects of wave grouping is also relevant in triggering breaking, which partly destroys the groups and transfers irreversible energy to low frequencies.

The main purpose of the following analysis is to understand how the presence of co- or counter-currents affects the grouping in the initial phases of the wind waves generation. Observing Figures 4–5 it is quite evident that grouping is present with well different characteristics depending on the velocity of the current and also on the speed of the wind.

Starting from the zero-crossing analysis, we can define a *run* as a group of consecutive waves exceeding a threshold value (see the insert in Figure 16*a*). The number of waves belonging to the group is the length of the run, j. The repetition length of waves is the number of waves between two starting waves of subsequent groups. Such a repetition of wave heights can be defined as a *total run*.

Longo [13] introduced new time and length scales that are related to the length of the run (which can be easily transformed in the period of the run and length of the group), and similar scales can be defined with reference to the total run length. Such scales can be important (i) for the analysis of the interaction between the air flow field and the water waves, and (ii) for any practical applications where the groups of waves represents a non-negligible forcing of the system, like reflection and vertical mixing.

Following Goda [55], the probability of a run with length j for uncorrelated waves is

$$P_u(j) = p_0^{j-1}(1 - p_0), \tag{10}$$

where p_0 is the occurrence probability that $H > H_t$ (H_t is the threshold wave

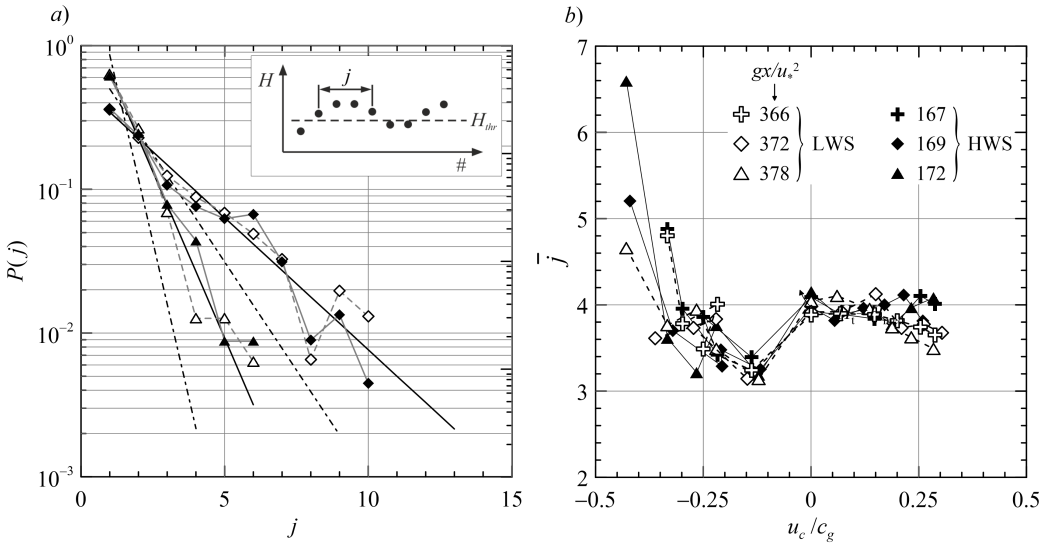

Figure 16: Groups properties. *a*) Distribution of the length of runs of high waves exceeding H_{med} and $H_{1/3}$, respectively, for tests without current. $H \geq H_{\mathrm{med}}$: $-\blacklozenge-$ test 22, HWS, $-\diamond-$ test 21, LWS, $-$ theory (correlated), $-.-$ theory (uncorrelated). $H \geq H_{1/3}$: $-\blacktriangle-$ test 22, HWS, $-\triangle-$ test 21, LWS. *b*) Mean length of runs of high waves exceeding H_{med} as a function of the current speed.

height), usually assumed of the Rayleigh form. Real waves are correlated and the previous equation underestimates the grouping. Hence, following Kimura [58] if we define p_{22} as the probability that H_2 exceeds H_t under the condition that the previous wave H_1 has already exceeded the threshold, the probability distribution of a run with length j for correlated waves is

$$P_c\left(j\right) = p_{22}^{j-1}\left(1 - p_{22}\right). \tag{11}$$

Again, p_{22} is usually computed by assuming a Rayleigh distribution of the wave height. Figure 16*a* shows the good agreement between experimental frequencies and theory for correlated waves, whilst the theoretical frequency of uncorrelated waves is an underestimation. Two different thresholds were chosen and compared, namely the median wave height H_{med} and $H_{1/3}$, and groups up to 11 waves are present with a threshold equal to H_{med}.

For the correlated waves, the expected mean length of the run is

$$\overline{j} = \frac{1}{1 - p_{22}}. \tag{12}$$

The experimental mean length of the runs are shown in Figure 16*b*. We notice that a co-current does not significantly change the value of $\overline{j}$ with respect to the no-current. Vice versa, a counter-current induces an initial reduction of the mean length and then favours a fast growth. The explanation partly relies in the strong modifications of the spectra due to a counter-current, although the power spectral density itself is a weak tool to predict correctly the mean length of runs of waves exceeding a threshold (see Elgar *et al.* [59]). The reduction of the mean length of the groups for weak counter-current, and the increment for stronger counter-current, is an indirect indication that instabilities are initially suppressed and then enhanced by the opposite current; the co-currents have negligible effects if they are weak, becoming more effective if they are strong, favouring a slight reduction of the mean length of runs.

Figure 17 shows the time and space evolution of the wave profiles for test 8 and 10, bothin counter-current, corresponding to high wave-steepness (panel *a*) and low wave-steepness (panel *b*), respectively. The groups destruction starting from US1 is evident for test 8, with small waves between high waves and with a disordered appearance. The groups structure is evident for test 10, with a progressive increment on the run length.

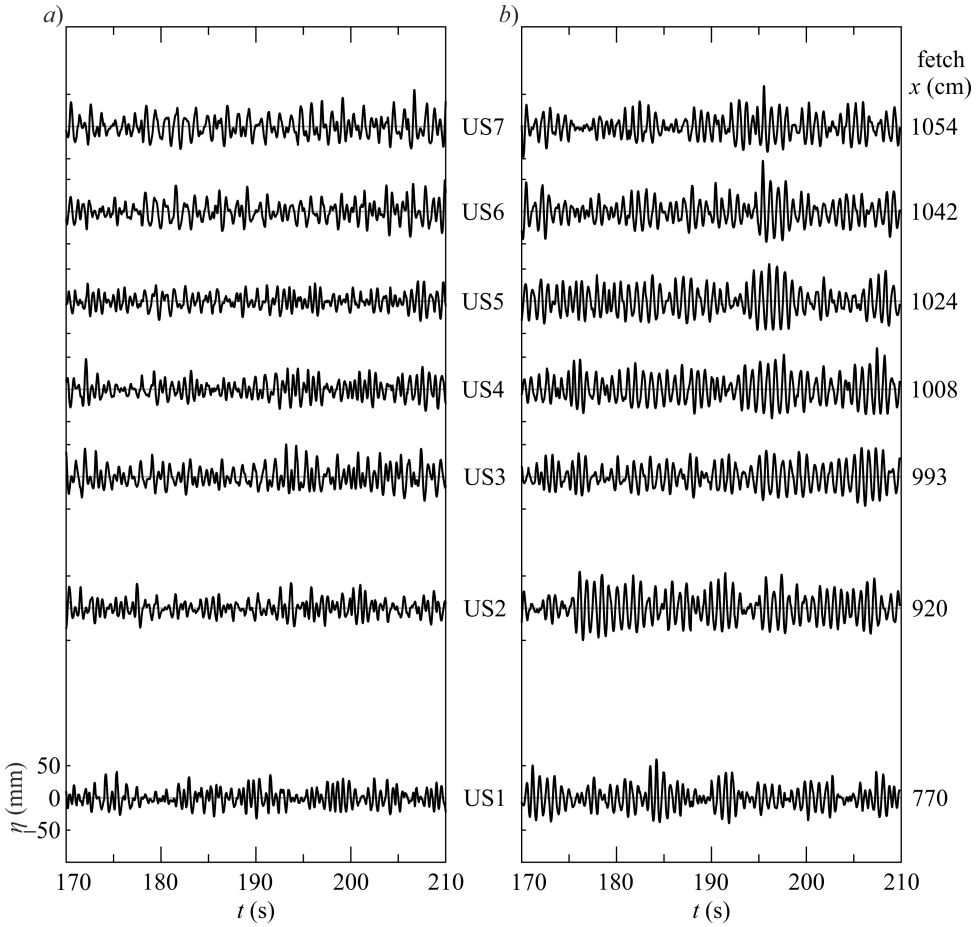

Figure 17: Example of the evolution of wave profiles. *a*) Test 08 with $u_c/c_g = -0.11$, HWS; *b*) Test 10 with $u_c/c_g = -0.26$, HWS.

5. Conclusions

A series of experiments conducted in a wind-wave tunnel with currents have revealed some peculiar aspects of the complex flow field. The complexity arises (i) from the non homogeneity, with energy progressively transferred by the wind, (ii) the shear action of the current, (iii) breaking, (iv) grouping and a mix of scales governing the process.

A co-current reduces the wave height growth with respect to the absence of current, with effects proportional to the current speed. It is a consequence of the reduction of the relative velocity (between air and water) with a reduction of the friction factor and of the efficiency of energy transfer. A counter-current generally breaks the monotonic growth of waves with fetch length, although the wave height is higher (in a given section and wind speed) than for an equal speed co-current. Part of the wave energy is dissipated by breaking (a micro-breaking is always expected at high wind speed), but the energy transfer from the wind is facilitated, hence the energy balance is still positive. The limited range of measurements prevents a clear-cut evidence, but we infer that the fetch section where wave height drop occurs is a function of the wind speed and of the current speed.

The wave steepness presents a maximum for weak counter-currents, decreasing both when co-current are present and when the counter-current becomes more intense. While in co-current the explanation is intuitive, since a decreasing wave height is accompanied by an increasing wave length, for counter-currents the interpretation relies on a wave length increasing faster than the wave height. Hence, an unexpected stabilization effect occurs in the latter configuration, which favours transferring of energy towards longer waves. This energy transfer is also evident in the spectral form, whose evolution is affected by both the energy input from the wind action and of the counter-current presence. A double-peak spectrum develops even for small values of u_c/c_g in counter-current.

Phase celerity is strongly influenced by the co-current presence, the stronger the current, the stronger the effects, whilst a counter-current does not have appreciable effects. The co-current condition always induces a strong increment of the phase celerity even with respect to theoretical models which include the current presence. We suspect that the discrepancy can be addressed to the continuous input of energy due to the blowing wind. We remind that the present experiments are in strong non homogeneous conditions and that increasing fetch length means higher energy transferred to the

waves.

Group celerity also experiences a strong variation with respect to the absence of current. We first notice that in absence of current, the group celerity of the wind waves increases faster than the phase celerity (increments are computed with respect to the group and phase celerity for the equivalent swell), with a ratio $(c_g - c_{g0})/(c - c_0) > 1.2$. The current acts in reducing this value, with a smooth decrease for co-current conditions and with dispersed data for counter-current conditions. The counter-current significantly reduces the flux of energy along the path, with a consequent fast increase of the wave height. In this respect the counter-current has a shoaling effect.

Grouping analysis reveals that the mean length of the group is almost unaffected by a co-current (unless the current itself is very strong), and is subject to non monotonic variations in presence of a counter-current. A minimum value of the length is observed in the counter-current domain, where a significant change in the wave field takes place. Larger speed of the counter-current favours longer wave groups.

Due to the complex and sometime unexpected phenomena, the overall scenario is sufficient to justify further tests aiming to a generalization of the present results. We bear in mind the small scale of the experiments, where, e.g,. the Weber number influence is neglected since tension surface effects are considered as negligible. Also, the finite size of the channel induces some extra-circulation which is included in bulk in the analysis, without a detailed separation of the wind drift, imposed current and secondary circulation. However, the results are clear cutting with respect to the profound difference between a co- and a counter-current.

Appendix A. Dimensional analysis for wind waves and currents and scaling

We consider the process of wave generation due to wind action, in the presence of a current. The general function can be written as

$$f\left(H_{rms}, T_p, u_*, F, t_d, g, u_c, h\right) = 0, \tag{A.1}$$

where H_{rms} is the root mean square wave height, T_p is the peak period, u_* is the friction velocity, F is the fetch length, t_d is the wind duration, g is the gravitational acceleration and u_c is a velocity scale of the current, h is the local depth. We are neglecting tension surface effects. The problem is

purely kinematic with a dimension of two, and upon selection of g and u_* as fundamental variables, dimensional analysis suggests a maximum of six non-dimensional groups, and eq.(A.1) reduces to

$$f\left(\frac{gH_{rms}}{u_*^2}, \frac{gT_p}{u_*}, \frac{u_c}{u_*}, \frac{gF}{u_*^2}, \frac{gt_d}{u_*}, \frac{gh}{u_*^2}\right) = 0. \tag{A.2}$$

Although friction velocity is considered a correct scale for growing waves characteristics [see, e.g., 60], the group celerity of the waves c_g seems more appropriate for the current effects, with the group u_c/u_* substituted by u_c/c_g. This last group can be introduced by mean of the dispersion relation for linear waves, which can be expressed as $f(c_g/u_*, gh/u_*^2, gT_p/u_*) = 0$. As a consequence of the different choice of the velocity scale, the general function (A.2) becomes

$$f\left(\frac{gH_{rms}}{u_*^2}, \frac{gT_p}{u_*}, \frac{u_c}{c_g}, \frac{gF}{u_*^2}, \frac{gt_d}{u_*}, \frac{gh}{u_*^2}\right) = 0. \tag{A.3}$$

As long as the waves are in deep water (the present experiments meet this condition), the group gh/u_* can be eliminated. In a similar way, if the duration of the wind is enough to saturate the given fetch, we are in stationary generation condition and also the group gt_d/u_* is not relevant. Overall, the general function in deep water and in stationary condition can be written as

$$f\left(\frac{gH_{rms}}{u_*^2}, \frac{gT_p}{u_*}, \frac{u_c}{c_g}, \frac{gF}{u_*^2}\right) = 0. \tag{A.4}$$

A relevant issue is related to the scaling between the experiments in the laboratory and the field. The approximate similarity is based on the Froude number, which forces a velocity and a time scale equal to $\lambda^{1/2}$, being λ the geometric scale. At the same time the Reynolds number, which is relevant mainly for the air flow, scales as $\lambda^{3/2}$ and assumes a smaller value in the laboratory than in the field, since $\lambda < 1$. It is a classical problem of scale effects, with air flow in the laboratory in a transition regime whereas is in a turbulent or fully turbulent regime in the field. For the wave flow, a Reynolds number based on the amplitude and on the orbital velocity of the waves [61] is

$$Re_w = \frac{aV}{\nu_w} = \frac{a^2\omega}{\nu_w}, \tag{A.5}$$

where a is the amplitude, $V = \omega a$ is the orbital velocity, ω is the pulsation, ν_w is the kinematic viscosity of water. Upon substitution of the dispersion relation, yields

$$Re_w = \sqrt{2g\pi}\frac{a^2}{\nu_w\sqrt{L}}, \tag{A.6}$$

where L is the local wave-length.The critical Reynolds number is $Re_{w,cr} \approx 3000$ and since the amplitude motion decays exponentially with depth, a similar decay is expected for Re_w, with a possibly turbulent flow near the free surface and a laminar flow beneath. This effect can be highly distorted in the laboratory, where the critical condition for turbulence is seldom reached also near the free surface, whereas it is a quite common condition in the field near the free surface and for a significant fraction of the water column. Note that this kind of turbulence is not related to wave breaking or to water drops accelerated by the wind before impacting the free surface [15]. Turbulence, once generated is diffused downwards by several other phenomena, and in the presence of currents can be also generated by the shear well beneath the free surface.

As for the air side, a relevant Reynolds number is based on a roughness length scale z_0:

$$Re_a = \frac{z_0 u_*}{\nu_a}, \tag{A.7}$$

where z_0 is defined as [62] $z_0 = \alpha u_*^2/g$, with $\alpha = 0.01 - 0.02$ the Charnock's parameter. The flow regime is considered aerodynamically rough (fully turbulent and not depending on air viscosity) if $Re_a >\approx 2.5$, and smooth if $Re_a <\approx 0.13$ [see, e.g., 63]. It is a matter of evidence that a reduction of the Reynolds number for the air in the laboratory can have the consequence of reproducing a transitional or even a smooth air flow, instead of a turbulent one.

All these information are a caveat for a correct extension of the laboratory results to the field. In particular, we expect that the laboratory experiments give an underestimation of the turbulence levels for the air and for the water, with a consequent underestimation of diffusivity of chemicals, gases, heat, with a limited spray generation, possibly with a generation of currents with velocity scaling not proportional to $\sqrt{\lambda}$ and with a different profile in the vertical.

In the present experiments $Re_w = 700 - 7000$ (see Table 1), with 10 tests (most in low wind speed - LWS - condition) in the transition regime;

the Reynolds number for the air side is $Re_a = 20 - 67$, always in turbulent regime. We expect that by extrapolating the laboratory results to field data with a geometric scale $\lambda \ll 1$, a scale effect is present for the water flow field.

References

[1] M. Sclavo, A. Benetazzo, S. Carniel, A. Bergamasco, F. M. Falcieri, D. Bonaldo, Wave-current interaction effect on sediment dispersal in a shallow semi-enclosed basin, Journal of Coastal Research 65 (sp2) (2013) 1587–1592.

[2] L. Chiapponi, S. Longo, E. Palmisani, C. De Piccoli, B. Matticchio, Wave-current interaction in the Porto di Lido entrance of the Venice Lagoon, in: Proceedings of the XXII TELEMAC-MASCARET Technical User Conference October 15-16, 2026, 2015, pp. 148–153.

[3] L. Melito, M. Postacchini, A. Sheremet, J. Calantoni, G. Zitti, G. Darvini, M. Brocchini, Wave-Current Interactions and Infragravity Wave Propagation at a Microtidal Inlet, in: Multidisciplinary Digital Publishing Institute Proceedings, Vol. 2(11), 2018, p. 628.

[4] O. M. Phillips, On the generation of waves by turbulent wind, Journal of Fluid Mechanics 2 (5) (1957) 417–445.

[5] J. W. Miles, On the generation of surface waves by shear flows, Journal of Fluid Mechanics 3 (2) (1957) 185–204.

[6] J. W. Miles, On the generation of surface waves by shear flows. part 4, Journal of Fluid Mechanics 13 (3) (1962) 433–448.

[7] O. M. Phillips, The dynamics of the upper ocean, Cambridge University Press, 1977.

[8] P. A. E. M. Janssen, Quasi-linear theory of wind-wave generation applied to wave forecasting, Journal of Physical Oceanography 21 (11) (1991) 1631–1642.

[9] J. W. Miles, Surface-wave generation revisited, Journal of Fluid Mechanics 256 (1993) 427–441.

[10] T. S. Hristov, S. D. Miller, C. A. Friehe, Dynamical coupling of wind and ocean waves through wave-induced air flow, Nature 422 (6927) (2003) 55.

[11] L. Grare, L. Lenain, W. K. Melville, Wave-coherent airflow and critical layers over ocean waves, Journal of Physical Oceanography 43 (10) (2013) 2156–2172.

[12] D. Liberzon, L. Shemer, Experimental study of the initial stages of wind waves' spatial evolution, Journal of Fluid Mechanics 681 (2011) 462–498.

[13] S. Longo, Wind-generated water waves in a wind tunnel: Free surface statistics, wind friction and mean air flow properties, Coastal Engineering 61 (1) (2012) 27–41. doi:10.1016/j.coastaleng.2011.11.008.

[14] S. Longo, D. Liang, L. Chiapponi, L. Aguilera Jimenez, Turbulent flow structure in experimental laboratory wind-generated gravity waves, Coastal Engineering 64 (2012) 1 – 15. doi:10.1016/j.coastaleng.2012.02.006.

[15] S. Longo, L. Chiapponi, M. Clavero, T. Mäkelä, D. Liang, Study of the turbulence in the air-side and water-side boundary layers in experimental laboratory wind induced surface waves, Coastal Engineering 69 (2012) 67–81.

[16] J. D. A. Van Hoften, S. Karaki, Interaction of waves and a turbulent current, in: Proceedings of Coastal Engineering 1976, ASCE, 1977, pp. 404–422.

[17] W. D. Grant, O. S. Madsen, Combined wave and current interaction with a rough bottom, Journal of Geophysical Research: Oceans 84 (C4) (1979) 1797–1808.

[18] P. H. Kemp, R. R. Simons, The interaction between waves and a turbulent current: waves propagating with the current, Journal of Fluid Mechanics 116 (1982) 227–250.

[19] P. H. Kemp, R. R. Simons, The interaction of waves and a turbulent current: waves propagating against the current, Journal of Fluid Mechanics 130 (1983) 73–89.

[20] J. Groeneweg, G. Klopman, Changes of the mean velocity profiles in the combined wave–current motion described in a GLM formulation, Journal of Fluid Mechanics 370 (1998) 271–296.

[21] J. F. A. Sleath, Velocities and shear stresses in wave-current flows, Journal of Geophysical Research: Oceans 96 (C8) (1991) 15237–15244.

[22] G. Klopman, Vertical structure of the flow due to waves and currents-laser-doppler flow measurements for waves following or opposing a current, WL report H840-30, part II, for Rijkswaterstaat.

[23] G. Klopman, Secondary circulation of the flow due to waves-laser-doppler flow measurements following or opposing a current, WL rapport Z2249 for Rijkswaterstaat.

[24] M. Umeyama, Reynolds stresses and velocity distributions in a wave-current coexisting environment, Journal of Waterway, Port, Coastal, and Ocean Engineering 131 (5) (2005) 203–212.

[25] J. A. Smith, Wave–current interactions in finite depth, Journal of Physical Oceanography 36 (7) (2006) 1403–1419.

[26] S. Roy, K. Debnath, B. S. Mazumder, Distribution of eddy scales for wave current combined flow, Applied Ocean Research 63 (2017) 170–183.

[27] A. Chawla, J. T. Kirby, Experimental study of wave breaking and blocking on opposing currents, in: Proceedings of Coastal Engineering 1998, ASCE, 1999, pp. 759–772.

[28] A. Chawla, J. T. Kirby, Monochromatic and random wave breaking at blocking points, Journal of Geophysical Research: Oceans 107 (C7) (2002) 4–1.

[29] I. K. Suastika, M. P. C. d. Jong, J. A. Battjes, Experimental study of wave blocking, in: Proceedings of Coastal Engineering 2000, ASCE, 2001, pp. 227–240.

[30] Y. Ma, G. Dong, M. Perlin, X. Ma, G. Wang, J. Xu, Laboratory observations of wave evolution, modulation and blocking due to spatially varying opposing currents, Journal of Fluid Mechanics 661 (2010) 108–129.

[31] S. R. Long, N. E. Huang, Observations of wind-generated waves on variable current, Journal of Physical Oceanography 6 (6) (1976) 962–968.

[32] Q. Zou, H. Chen, Wind and current effects on extreme wave formation and breaking, Journal of Physical Oceanography 47 (7) (2017) 1817–1841.

[33] M. Onorato, D. Proment, A. Toffoli, Triggering rogue waves in opposing currents, Physical Review Letters 107 (18) (2011) 184502.

[34] T. Waseda, T. Kinoshita, L. Cavaleri, A. Toffoli, Third-order resonant wave interactions under the influence of background current fields, Journal of Fluid Mechanics 784 (2015) 51–73.

[35] A. Toffoli, L. Cavaleri, A. Babanin, M. Benoit, E. Bitner-Gregersen, J. Monbaliu, M. Onorato, A. R. Osborne, C. Stansberg, Occurrence of extreme waves in three-dimensional mechanically generated wave fields propagating over an oblique current, Natural Hazards and Earth System Sciences 11 (3) (2011) 895–903.

[36] Y. Ma, X. Ma, M. Perlin, G. Dong, Extreme waves generated by modulational instability on adverse currents, Physics of Fluids 25 (11) (2013) 114109.

[37] A. Toffoli, T. Waseda, H. Houtani, T. Kinoshita, K. Collins, D. Proment, M. Onorato, Excitation of rogue waves in a variable medium: An experimental study on the interaction of water waves and currents, Physical Review E 87 (5) (2013) 051201.

[38] A. Toffoli, T. Waseda, H. Houtani, L. Cavaleri, D. Greaves, M. Onorato, Rogue waves in opposing currents: an experimental study on deterministic and stochastic wave trains, Journal of Fluid Mechanics 769 (2015) 277–297.

[39] G. Rousseaux, C. Mathis, P. Maïssa, T. G. Philbin, U. Leonhardt, Observation of negative-frequency waves in a water tank: a classical analogue to the Hawking effect?, New Journal of Physics 10 (5) (2008) 053015.

[40] K. F. Lambrakos, Wave-current interaction effects on water velocity and surface wave spectra, Journal of Geophysical Research: Oceans 86 (C11) (1981) 10955–10960.

[41] J. Wolf, D. Prandle, Some observations of wave–current interaction, Coastal Engineering 37 (3-4) (1999) 471–485.

[42] A. J. van der Westhuysen, Spectral modeling of wave dissipation on negative current gradients, Coastal Engineering 68 (2012) 17–30.

[43] M. Viitak, I. Maljutenko, V. Alari, Ü. Suursaar, S. Rikka, P. Lagemaa, The impact of surface currents and sea level on the wave field evolution during St. Jude storm in the eastern Baltic Sea, Oceanologia 58 (3) (2016) 176–186.

[44] Z. Wei, R. A. Dalrymple, M. Xu, R. Garnier, M. Derakhti, Short-crested waves in the surf zone, Journal of Geophysical Research: Oceans 122 (5) (2017) 4143–4162.

[45] T. S. Hedges, R. G. Tickell, J. Akrigg, Interaction of short-crested random waves and large-scale currents, Coastal Engineering 19 (3-4) (1993) 207–221.

[46] L. Cavaleri, J.-H. Alves, F. Ardhuin, A. Babanin, M. Banner, K. Belibassakis, M. Benoit, M. Donelan, J. Groeneweg, T. Herbers, P. Hwang, P. Janssen, T. Janssen, I. Lavrenov, R. Magne, J. Monbaliu, M. Onorato, V. Polnikov, D. Resio, W. Rogers, A. Sheremet, J. M. Smith, H. Tolman, G. van Vledder, J. Wolf, I. Young, Wave modelling – The state of the art, Progress in Oceanography 75 (4) (2007) 603 – 674. doi:https://doi.org/10.1016/j.pocean.2007.05.005.

[47] K. Hasselmann, T. P. Barnett, E. Bouws, H. Carlson, D. E. Cartwright, K. Enke, J. A. Ewing, H. Gienapp, D. E. Hasselmann, P. Kruseman, A. Meerburg, P. Mullar, D. J. Olbers, K. Richter, W. Sell, H. Walden, Measurements of wind-wave growth and swell decay during the Joint North Sea Wave Project (JONSWAP), Ergänzungsheft 8-12.

[48] M. S. Longuet-Higgins, R. W. Stewart, The changes in amplitude of short gravity waves on steady non-uniform currents, Journal of Fluid Mechanics 10 (4) (1961) 529–549.

[49] M. P. Tulin, T. Waseda, Laboratory observations of wave group evolution, including breaking effects, Journal of Fluid Mechanics 378 (1999) 197–232.

[50] V. Zakharov, N. Filonenko, Energy spectrum for stochastic oscillations of the surface of a liquid, in: Soviet Physics Doklady, Vol. 11, 1967, p. 881.

[51] P. Denissenko, S. Lukaschuk, S. Nazarenko, Gravity wave turbulence in a laboratory flume, Physical review letters 99 (1) (2007) 014501.

[52] L. Deike, B. Miquel, P. Gutiérrez, T. Jamin, B. Semin, M. Berhanu, E. Falcon, F. Bonnefoy, Role of the basin boundary conditions in gravity wave turbulence, Journal of Fluid Mechanics 781 (2015) 196–225.

[53] A. Toffoli, D. Proment, H. Salman, J. Monbaliu, F. Frascoli, M. Dafilis, E. Stramignoni, R. Forza, M. Manfrin, M. Onorato, Wind generated rogue waves in an annular wave flume, Physical Review Letters 118 (14) (2017) 144503.

[54] J. S. Bendat, A. Piersol, Random Data Analysis and Measurement Procedures, Wiley, 2000.

[55] Y. Goda, Random seas and design of maritime structures, Vol. 33, World Scientific Publishing Company, 2010.

[56] M. Smith, E. Poulter, J. McGregor, Doppler radar measurements of wave groups and breaking waves, Journal of Geophysical Research: Oceans 101 (C6) (1996) 14269–14282.

[57] T. Waseda, M. P. Tulin, Experimental study of the stability of deep-water wave trains including wind effects, Journal of Fluid Mechanics 401 (1999) 55–84.

[58] A. Kimura, Statistical properties of random wave groups, in: Proceedings of Coastal Engineering 1980, ASCE, 1980, pp. 2955–2973.

[59] S. Elgar, R. T. Guza, R. J. Seymour, Groups of waves in shallow water, Journal of Geophysical Research: Oceans 89 (C3) (1984) 3623–3634.

[60] P. Janssen, G. Komen, W. De Voogt, Friction velocity scaling in wind wave generation, Boundary-Layer Meteorology 38 (1-2) (1987) 29–35.

[61] A. V. Babanin, On a wave-induced turbulence and a wave-mixed upper ocean layer, Geophysical Research Letters 33 (20).

[62] H. Charnock, Wind stress on a water surface, Quarterly Journal of the Royal Meteorological Society 81 (350) (1955) 639–640.

[63] E. B. Kraus, J. A. Businger, Atmosphere-ocean interaction, Vol. 27, Oxford University Press, 1994.